



Priming mechanisms with additions of pyrogenic organic matter to soil

Silene DeCiucies^a, Thea Whitman^b, Dominic Woolf^a, Akio Enders^a,
Johannes Lehmann^{a,c,*}

^a *Soil and Crop Sciences, School of Integrative Plant Science, Cornell University, Ithaca, NY 14850, USA*

^b *Department of Soil Science, University of Wisconsin, Madison, WI 53706, USA*

^c *Atkinson Center for a Sustainable Future, Cornell University, Ithaca, NY 149850, USA*

Received 10 April 2018; accepted in revised form 4 July 2018; Available online 11 July 2018

Abstract

Additions of pyrogenic organic matter (PyOM) to soil have been shown to both increase and decrease mineralization of native soil organic carbon (nSOC). This change in mineralization rate is referred to as priming, and may have important implications for carbon (C) turnover in soil. This study quantifies both positive and negative priming mechanisms using high-resolution carbon dioxide (CO₂) measurements using a series of short-term incubation experiments with ¹³C-labeled PyOM added to a temperate forest soil. Moisture, nutrient availability and pH were adjusted to minimize any differential effects on nSOC mineralization. Irrespective of pyrolysis temperature (200–750 °C), addition of 10 mg PyOM g⁻¹ soil significantly decreased mineralization of nSOC. Dilution was measured against inorganic bulking materials with different surface areas and accounted for 19% of negative priming observed at day 7, and 13% at day 35. In comparison, substrate switching caused only 1% of negative priming assumed to be equivalent to PyOM mineralization itself. Inhibition did not explain reductions in nSOC mineralization since the microbial biomass did not significantly decrease ($p > 0.05$). Sorptive protection of dissolved organic carbon (DOC) was responsible for the majority of negative priming observed with PyOM additions based on adsorption isotherm experiments as well as co-location of nSOC on PyOM surfaces shown by nanoSIMS. Maximum sorption of soil DOC was 29 times higher to PyOM pyrolyzed at 450 °C than to topsoil, and tripled with an increase in pyrolysis temperature to 750 °C. This tripling in DOC sorption potential to PyOM produced at 750 °C in comparison to 450 °C was only reflected in a less than twice lower nSOC mineralization. Sorptive protection was with 80% the dominant negative priming mechanism on monthly timescales and likely beyond. These results have implications for long-term SOC storage, because sorption has more persistent effects than substrate switching or dilution.

© 2018 Elsevier Ltd. All rights reserved.

Keywords: Biochar; Pyrogenic organic matter; Nano-SIMS; Carbon sequestration; Priming

1. INTRODUCTION

Within the global carbon (C) cycle, soil organic C (SOC) represents a substantial pool of over 2000 Pg C (Ciais et al., 2013). SOC is not only a large C pool – it is also very dynamic, being sustained by large inputs of plant litter that, under equilibrium conditions, compensate for an equally large microbial mineralization of SOC to carbon dioxide

* Corresponding author at: Soil and Crop Sciences, School of Integrative Plant Science, Cornell University, Ithaca, NY 14850, USA.

E-mail address: CL273@cornell.edu (J. Lehmann).

(CO₂) of about 60 Pg yr⁻¹ (Ciais et al., 2013). These two factors give SOC great potential to affect atmospheric CO₂, because soils contain three times more C than the atmosphere or terrestrial vegetation (Stockmann et al., 2013), and small fractional changes to SOC stocks have therefore proportionally large effects on the global C cycle.

One important avenue through which SOC pools are affected is priming (Bingeman et al., 1953; Kuzyakov, 2010). Priming is defined here as a change in mineralization rate of already-present (native) SOC caused by additions of new organic matter. It can be positive (the mineralization of native SOC (nSOC) increases), or negative (nSOC mineralization decreases) (Bingeman et al., 1953). Recently, the input of pyrogenic organic matter (PyOM) as a result of vegetation fires (Lehmann et al., 2008) or deliberate additions in the form of biochar (Laird, 2008) have received increasing attention with regard to priming of SOC. With climate change, fire activity is increasing globally (Abatzoglou and Williams, 2016; Williams and Abatzoglou 2016), accelerating the deposition of PyOM. PyOM is already ubiquitous in soil, but with these changes, its presence may increase over time (Bird et al., 2015; Santín et al., 2016), which makes priming elicited by PyOM an increasingly relevant process. However, the contribution of mechanisms responsible for nSOC mineralization either increasing or decreasing under different conditions remains poorly quantified (Wang et al., 2016).

Potential mechanisms (Maestrini et al., 2015; Whitman et al., 2015) for positive priming as a result of PyOM include: (i) *co-metabolism*: microbial decomposition of easily mineralizable PyOM fractions increases microbial activity, and facilitates additional decomposition of nSOC by active enzymes; (ii) *stimulation*: PyOM additions may result in improved pH, nutrient, oxygen, or water contents as well as general habitat for soil biota resulting in increased microbial activity. Negative priming may be a result of: (i) *inhibition*: the opposite of stimulation, whereby constraints are aggravated by substrate addition, as well as by inorganic or organic substances in PyOM, which directly inhibit microbial activity. PyOM addition may also cause inhibition by interfering with the functions of enzymes or signaling compounds; (ii) *substrate switching*: easily-mineralizable fractions of PyOM additions are preferentially used by microbes, causing a decrease in nSOC mineralization; (iii) *dilution*: addition of PyOM that is largely not metabolized temporarily dilutes more or equally microbially favorable nSOC through physical dilution; (iv) *induced aggregation*: PyOM encourages aggregation whereby C may be protected and stored for a longer period of time; (v) *sorption*: organic compounds are sorbed by PyOM, decreasing their rate of mineralization through e.g. cation bridging.

Of the above mechanisms, individual ones have been explored in recent studies with PyOM and SOC in isolation, without an attempt to compare their quantitative importance more comprehensively. Substrate switching has been proposed to be associated primarily with short-term priming through additions of easily mineralizable OM substrates (Whitman et al., 2014b), but has not

been quantitatively compared with other mechanisms. Inhibition has been suggested not to apply to PyOM due to the lack of observed effects on microbial biomass (Maestrini et al., 2014). Dilution was proposed as a possible mechanism (Whitman et al., 2014b), yet its quantitative importance and duration remains unexplored. Sorption has been proposed as a dominant negative priming mechanism in various studies (Cross and Sohi 2011; Kuzyakov et al., 2009; Maestrini et al., 2014; Whitman et al., 2014b; Zimmerman et al., 2011) due to PyOM's high surface area, porosity, charge, and overall adsorptive nature, but not compared to other mechanisms.

Various studies have been conducted on the net priming effects of PyOM on SOC, yielding a wide array of responses (Maestrini et al., 2015; Whitman et al., 2015; Wang et al., 2016), and emphasize the need for mechanistic studies that can help in understanding priming mechanisms within different environments. Microbial biomass and activity often increase after additions of PyOM (Lehmann et al., 2011) indicating that direct microbial toxicity is unlikely to play a role for most PyOM materials. Yet such changes may still either reduce nSOC mineralization by substrate switching or increase nSOC mineralization by co-metabolism, the net effect being uncertain. It is clear that soil type (Luo et al., 2011; Keith et al., 2011), nSOC properties (Cross and Sohi, 2011; Whitman et al., 2014b), soil temperature (Fang et al., 2015) and the presence of plants (Keith et al., 2015; Weng et al., 2017; Whitman et al., 2014a) play important roles. While many of these studies have a limited ability to comprehensively identify mechanisms, it is clear that different PyOM properties have significant effects on priming that may even change over short periods of time (Zimmerman et al., 2011). Many of the changes in nSOC mineralization induced by priming occur over periods of weeks to months (Wardle et al., 2008; Whitman et al., 2014a, 2014b; Zimmerman et al., 2011) and likely involve several mechanisms operating simultaneously with changing intensity over time. A comprehensive assessment of priming effects by PyOM with high temporal resolution that would allow attribution of the different mechanisms has not been done.

This study investigates key mechanisms of priming by additions of PyOM. Specifically, the objectives include (1) simultaneous assessment of the contributions by positive and negative priming including inhibition (by toxicity), substrate switching, dilution, co-metabolism, and adsorption; (2) quantification of the rapid temporal changes in priming mechanisms operating during the period immediately following PyOM input to soil; (3) assessment of temporal changes of priming mechanisms over the course of several months.

We hypothesized that (i) dilution is not a significant mechanism in causing negative priming, and is restricted to short time scales; (ii) inhibition by direct OM toxicity is not a significant mechanism for priming; (iii) substrate switching or co-metabolism are short-term and therefore not quantitatively important mechanisms in response to PyOM additions; and (iv) sorption is the most important negative priming mechanism for PyOM.

2. MATERIALS AND METHODS

2.1. Methodological approach

This study utilizes a series of mineralization experiments with treatment combinations that allow separate quantification of positive and negative priming mechanisms through (1) adding inorganic materials of different surface areas (ashed subsoil, perlite, and quartz sand) but volume equivalent to the PyOM added; (2) increasing the pyrolysis temperature that enhances surface area and reduces the rapidly mineralizable fraction; and (3) varying the rate of application. Isotopic labeling of PyOM in combination with daily measurements of CO₂ emissions and one-time measurement of microbial biomass as well as their isotopic composition allows quantification of the contribution of priming mechanisms at high temporal resolution. These incubation experiments are complemented by adsorption experiments and imaging of the isotope composition on PyOM surfaces at high spatial resolution. Various parameters that are known to influence nSOC mineralization and would interfere with identification of the mechanisms hypothesized, were controlled for, such as by adjusting the pH of the mixtures to the pH of the soil, adding sufficient nutrients to compensate for any nutrient additions or nutrient immobilization by the PyOM, and adjusting the soil moisture content to the same matric potential (see detailed description in Section 2.7).

2.2. Biomass production

Two sets of Preble shrub willow (*Salix viminalis* × *S. miyabeana*) were grown concurrently, one in a greenhouse under ambient CO₂, the other in a growth chamber enriched with ¹³CO₂. Natural abundance δ¹³C willow was grown as a diluent for the valuable labeled willow used in the incubation studies. These were mixed to provide a δ¹³C in the range of 200–400‰ in those incubations where nanoSIMS analyses were not conducted. Samples for nanoSIMS analysis used unadulterated ¹³C enriched biomass. Unlabeled materials were used for characterization (Table 1; except for isotope contents). Both sets were grown in Cornell potting mix (Boodley and Sheldrake, 1972) from 0.3 m willow cuttings from the Cornell University Willow Research Farm in Geneva, NY. Plants were watered every 2nd day and fertilized weekly. An 18-hour photoperiod was maintained in Percival AR 100L3 growth chambers (Percival, Perry, IA, USA). Day and night temperatures were 24 and 17 °C, respectively, and humidity was maintained around 30–50% RH using a de-humidifier. Plants were fertilized with a modified Hoagland Solution (Whitman et al., 2014a) where N was supplied with ¹⁵N-ammonium sulfate (10 atom% ¹⁵N). Photoperiod CO₂ was maintained at 400 ppm. A portion of CO₂ enrichment was provided by 20 L of ¹³CO₂ (99 atom %). This was delivered only during the central 16 h of the photoperiod, and only after buds emerged from the cuttings. Labeled gas was metered with a peristaltic pump via a multilayer polyethylene and nylon

bag at atmospheric pressure. Plants were coppiced, leaving 2–3 nodes, three times over the 6 month growth period. Harvested material was separated into stems and leaves, and oven dried at 70 °C.

2.3. PyOM production and analyses

Oven-dried willow stems were milled to <2 mm before pyrolysis in a modified muffle furnace (Guerena et al., 2015). Samples were heated at 2.5 °C min⁻¹ to a target temperature of 200, 300, 450, 600, and 750 °C (Table 1), which was maintained for 30 min. The furnace was then cooled to ambient with a water heat exchanger. Argon gas ensured an anoxic environment during the entire heating and cooling process. To prepare for incubations, PyOM was shaken in deionized (DI) water overnight and rinsed to remove easily-soluble ash and water-soluble material. All PyOM was pH-adjusted to the pH of the soil used in the incubation (4.89) over the course of several days using 1 M HCl. Once the target pH was reached, PyOM was filtered, oven dried at 70 °C and sieved to 150–850 μm.

Ash, volatile matter, and fixed carbon in PyOM and the biomass it was produced from was assessed by proximate analysis according to Enders et al. (2012). Nitrate (NO₃⁻) and ammonium (NH₄⁺) were extracted with 2 M KCl and quantified on a continuous flow analyzer (Bran and Luebbe Autoanalyzer, SPX, Charlotte, NC). Dissolved organic carbon (DOC) was measured using a DOC analyzer (Shimadzu TOC-5000A, Columbia, MD, USA) following water extraction using a 1:20 (w/v) ratio that was shaken for 1 h at 100 min⁻¹, then filtered (0.45 μm glass fiber filter; GC-50, Advantec, Tokyo, Japan). Total C, nitrogen (N), hydrogen (H), and oxygen (O), bulk δ¹³C and δ¹⁵N were measured using a Delta V Isotope Ratio Mass Spectrometer (Thermo Scientific, Germany) coupled to a dry combustion analyzer (Carlo Erba NC2500 Elemental Analyzer, Italy). Inorganic C was assessed using the Bernard calcimeter gas displacement method (Nelson and Sommers, 1996). Total phosphorous (P) was assessed by Inductively Coupled Plasma Optical Emission Spectrometry (ICP-OES, iCAP 6000 series, Thermo Fisher Scientific, MA, USA) after preparation as per Enders and Lehmann (2012). Briefly, PyOM and biomass was dry ashed at 500 °C for 8 h, followed by wet digestion in concentrated nitric acid (HNO₃) and 30% hydrogen peroxide (H₂O₂) at 120 °C. Cation exchange capacity (CEC) was determined using the method of Graber et al. (2017), and pH was determined in DI water using a glass electrode (detection limit of 0.01 pH units) with a PyOM:water ratio of 1:10 (w/v) (Orion 3-Star pH Benchtop; Thermo Electron Corporation, Beverly, MA, USA) according to Singh et al. (2017). Specific surface area (SSA) was quantified using the B.E.T. method with CO₂ at 273.15 K and N₂ at 77.039 K (ASAP 2020, Micromeritics, Atlanta, GA, USA) (see Supplementary Discussion note).

Supplementary data associated with this article can be found, in the online version, at <https://doi.org/10.1016/j.gca.2018.07.004>.

Table 1
Properties of PyOM and the original uncharred biomass.

Property (units)	Biomass	PyOM				
		200 °C	300 °C	450 °C	600 °C	750 °C
Ash (%)	0.63	n/a ^a	1.63	1.87	2.92	2.72
Volatile matter (%)	92.52	86.90	49.17	23.86	13.99	10.48
Fixed carbon (%)	6.85	13.51	49.20	74.27	83.09	86.80
pH (H ₂ O) ^b	5.38	5.84	9.57	10.77	12.13	12.64
Extractable NO ₃ ⁻ and NO ₂ ⁻ (mg NO ₃ + NO ₂ -N kg ⁻¹)	11.60	9.96	1.02	1.06	0.88	0.64
Extractable NH ₄ ⁺ (mg NH ₄ -N kg ⁻¹)	106.84	19.80	12.15	15.12	6.18	6.32
Water extractable C (DOC) (mg kg ⁻¹)	5776.0	2343.9	478.7	275.4	75.8	102.5
Total H (%)	6.91	10.27	5.13	3.17	2.00	1.00
Total O (%)	47.84	72.63	21.79	12.78	9.23	7.22
Total C (%)	56.02	46.02	67.21	76.49	80.67	81.83
Inorganic C (%)	0.00	0.00	0.00	0.00	0.00	0.00
Total N (%)	1.77	1.60	2.91	3.05	2.64	2.60
Total P (mg kg ⁻¹)	338.2	242.0	981.7	1965.1	2821.0	3050.9
C/N (w/w)	31.6	28.9	23.1	25.1	30.6	31.47
H/C _{organic} (mol/mol)	1.47	2.67	0.91	0.50	0.30	0.15
O/C _{organic} (mol/mol)	0.64	1.18	0.24	0.13	0.09	0.07
Bulk ¹⁵ N (atom %)	8.19	7.81	8.07	7.95	8.00	8.02
Bulk ¹³ C (‰)	748.11	755.66	749.04	693.56	749.85	749.85

^a Not available.

^b Before pH adjustment to the pH of the soil (which minimized effects of pH on priming).

2.4. Preparation of additional amendments

Quartz sand (150–200 μm, U.S. Silica, Frederick, MD, USA), perlite, (Lambert, Quebec, CA) and subsoil (B-horizon of soil used in incubation) were sieved to 150–850 μm and ashed in a modified muffle furnace for 8 h at 500 °C to be used in the dilution incubation experiment. SSA was quantified using the B.E.T. method with N₂ at 77.039 K (ASAP 2020, Micromeritics, Atlanta, GA, USA).

2.5. Soils

Soil was collected from a mixed deciduous forest on Mt. Pleasant in Dryden, NY, at 42.460601, -76.387078 (Whitman et al., 2014b). The soil is a Mardin channery silt

loam, a coarse loamy, mixed, active, mesic typic Fragiudept that has had no instance of burning in recorded history (Table 2). For this set of incubations, the topsoil (0.02–0.2 m) horizon was collected after removing the O-horizon material. Field capacity of each soil mixture (soil + amendment) was determined (method modified from Black et al., 1965) in plastic tubing with an inner diameter matching that of the 60 mL Qorpak jar used in the incubations. Particle size fractionation and texture analysis was done according to Kettler et al. (2001). NO₃⁻ and NH₄⁺, total C, N, H, and O, bulk ¹³C and ¹⁵N, pH, and total nutrient contents were measured as described above for PyOM. Water soluble C (DOC) was extracted in DI H₂O using a 1:10 ratio (w/v), shaken for 1 h, filtered, and analyzed using the same method as PyOM.

Table 2
Properties of the studied soil.

Property (units)	Temperate Mardin Topsoil
Sand (%)	15.9
Silt (%)	59.5
Clay (%)	24.6
Texture (USDA classification)	Silt loam
Field capacity (mL g ⁻¹ soil)	0.82
Extractable NO ₃ ⁻ and NO ₂ ⁻ (mg NO ₃ + NO ₂ -N kg ⁻¹)	3.99
Extractable NH ₄ ⁺ (mg NH ₄ -N kg ⁻¹)	45.7
Water-extractable C (DOC) (mg kg ⁻¹)	704
Total C (%)	5.28
Total N (%)	0.38
Bulk ¹³ C (‰)	-27.4
Bulk ¹⁵ N (‰)	1.22
C/N (g g ⁻¹)	13.90
pH (H ₂ O)	4.89

2.6. Adsorption isotherms

Adsorption isotherms were generated for some of the original materials, namely topsoil, ashed subsoil, PyOM produced at either 450 °C or 750 °C. The DOC for this adsorption experiment was obtained by shaking the topsoil in DI water for 2 h, then centrifuging and filtering the soil slurry through a 0.45- μm glass fiber filter (GC-50, Advantec, Tokyo, Japan). The DOC was diluted to 7 concentrations (0, 10, 20, 50, 80, 100 and 160 mg g^{-1}) and each dilution was shaken with 0.5 g adsorbent (either the topsoil, ashed subsoil, PyOM produced at either 450 °C or 750 °C; all before incubation) for 12 h before centrifugation (2000 rpm for 10 min), filtration, and analysis. Filtrates and original DOC extracts were analyzed using a Shimadzu TOC analyzer (Shimadzu TOC-5000A, Columbia, MD, USA).

2.7. Incubation experiments

2.7.1. General conditions for all three incubation experiments

All three incubations took place in 1-L Mason jars. Thirty mL DI water was maintained in the bottom of each jar to maintain 100% humidity and each jar contained a smaller 60-mL Qorpak bottle with 40 g wet soil + amendment mixture. Dry topsoil and dry amendments or the topsoil on its own (as a control) were added to the bottles, mixed, and water was added to achieve 65% field capacity for the soil + amendment mixture in order to minimize differential moisture availability as a factor influencing mineralization. One mL of a modified Hoagland solution was added to each jar to supply sufficient nutrients to minimize any effects of nutrients added with the PyOM (Whitman et al., 2014b). The pH of each incubation was adjusted to the pH of the control soil without additions in order to minimize the effect of pH (Whitman et al., 2014b). Each treatment was replicated 5 times. Incubations were continuously monitored using a Picarro CO₂ stable isotope analyzer (G2201-I, Santa Clara, CA, USA) fitted with a custom-built sequential-multiplexing manifold capable of sampling 112 microcosms, with headspace gas recycled from the CO₂ analyzer back through the Mason jars. Headspace gas from each sample jar was sampled for 6 min during each sampling period, and subsequently purged with CO₂-free air. Data were collected at a rate of two measurements s⁻¹ over the 6-min sampling period, and also throughout the 6-min sample purge in order to record the baseline values before each cycle's respiration measurements.

2.7.2. Experiment 1: Volumetric dilution

The PyOM (450 °C) was added to soil at 10 mg g^{-1} in comparison to different bulking amendments to assess the effect of dilution on SOC mineralization. Ashed subsoil, perlite, and quartz sand were added to soil at an equivalent bulk volume to the PyOM addition (1.36 $\text{cm}^3 \text{ jar}^{-1}$) to achieve the same amount of physical dilution but with different surface areas (see supplementary online Table S1). Each treatment was replicated five times. The samples were incubated for 35 d and were measured for CO₂ and its ¹³C isotope content 84 times over the duration of the incubation.

2.7.3. Experiment 2: Pyrolysis temperature

The PyOM produced at different temperatures (200, 300, 450, 600, 750 °C) was added to soil at a rate of 10 mg g^{-1} . Each treatment was replicated five times. The samples were incubated for 62 d and respired CO₂ was sampled daily.

2.7.4. Experiment 3: Application rate

The PyOM (450 °C) was added to soil at rates of 0 (control), 0.5, 1, 2.5, 5, and 10 mg g^{-1} dry soil. Each treatment was replicated five times. The samples were incubated for 35 days and sampled daily for CO₂ and its ¹³C isotope content.

2.8. Microbial biomass

At the conclusion of the incubation of Experiment 2 (Pyrolysis temperature), microbial biomass was measured only in soil with PyOM pyrolyzed at 300, 450, or 750 °C in comparison to soil alone by chloroform (CHCl₃) fumigation extraction, using a modified method of Witt et al. (2000) described in Liang et al. (2010). In brief, 20 mL of 0.05 M K₂SO₄ was added to 15 g wet soil for extraction and shaken on a low-speed reciprocal shaker for 4.5 h. Ethanol-free CHCl₃ (1 mL) was added to a separate set during extraction to lyse the microbes generating one set that was fumigated and one set that was not fumigated. The extracts were centrifuged at 4000 rpm for 10 min and the supernatant filtered through a No. 41 Watman filter paper. The extracts were dried at 50 °C and analyzed for isotopic C concentrations using the modified method from Bruuslema and Duxbury (1996). Dried K₂SO₄ salt extracts were analyzed for total C and $\delta^{13}\text{C}$ using a Delta V Isotope Ratio Mass Spectrometer (Thermo Scientific, Germany) coupled to a Carlo Erba NC2500 Elemental Analyzer (Italy). An extraction efficiency coefficient of 0.45 was used to determine the total microbial biomass (Vance et al., 1987; Jenkinson et al., 2004), C recovered by the unfumigated control was subtracted, and 2-part $\delta^{13}\text{C}$ partitioning was used to attribute the microbial biomass C (MB-C) source to either nSOC or PyOM using the equation:

$$f_{\text{PyOM-MB-C}} = (\delta_{\text{MB-C-Total}} - \delta_{\text{nSOC}}) / (\delta_{\text{PyOM}} - \delta_{\text{nSOC}}),$$

where $f_{\text{PyOM-MB-C}}$ represents the fraction of MB-C from PyOM, $\delta_{\text{MB-C-Total}}$, δ_{nSOC} , and δ_{PyOM} represent the $\delta^{13}\text{C}$ signatures of the total MB-C, nSOC, and PyOM, respectively (Balesdent and Mariotti, 1996). $\delta_{\text{MB-C-Total}}$ was calculated from the $\delta^{13}\text{C}$ signatures of fumigated and unfumigated control as well as the C extracted using a simple mixing model. After microbial biomass extraction, soils were air-dried and sealed in air-tight storage bottles.

2.9. NanoSIMS

NanoSIMS images were collected for incubated PyOM particles (only 450 °C and 600 °C) from Experiment 2 (Pyrolysis temperature) at the Environmental Molecular Sciences Laboratory at the Pacific Northwest National Laboratory in Richland, WA, USA (Cameca NanoSIMS 50L spectrometer, AMETEK Inc., CAMECA SAS, Paris, France). To prepare samples after incubation for

nanoSIMS analyses, air-dried intact micro-aggregates (100–400 μm) were broken open using an X-ACTO knife to expose an interior surface along pore spaces within the aggregate. Once the aggregate was opened, a visible PyOM particle was removed using super tweezers and was placed on the sample holder. Also unincubated PyOM (only 450 $^{\circ}\text{C}$) was mounted in this way. Two methods for fixing the PyOM particle onto a sample holder for nanoSIMS imaging were included to reduce biases and results allowed identical conclusions: (a) The PyOM particle was pressed into indium foil using a glass microscope slide. (b) Particles were embedded in Field's metal (ESPI Metals, Ashland, OR, USA) by dropping the sample into molten metal at 60 $^{\circ}\text{C}$ and quickly covering it with a glass microscope slide so that the top of the sample and Field's metal were completely flat. Samples were then sputter coated in $\sim 5 \mu\text{m}$ high-purity iridium to improve conductivity and imaged with a scanning electron microscope followed by nanoSIMS. Negative secondary gallium ions were accelerated to 8 keV and were simultaneously counted using electron multipliers. The magnetic field was stabilized using NMR regulation and secondary ion peaks were monitored throughout the day and adjusted for drift. Prior to image analysis, image areas were pre-sputtered with about 2×10^{16} ions cm^{-2} . Ion images of $^{12}\text{C}_2^-$, $^{12}\text{C}^{13}\text{C}^-$, $^{12}\text{C}^{14}\text{N}^-$, $^{12}\text{C}^{15}\text{N}^-$, $^{28}\text{Si}^-$, $^{31}\text{P}^-$, and $^{32}\text{S}^-$ were collected using a 1.5 pA, primary beam that had a diameter of approximately 120 nm and a dwell time of 13.5 ms pixel^{-1} . Each $45 \mu\text{m} \times 45 \mu\text{m}$ image consisted of two 256×256 pixel frames (175-by-175 nm).

Images were processed using ImageJ software with the open-MIMS plug-in for Fiji (nano.bwh.harvard.edu/MIMSSoftware). Images were corrected for deadtime and QSA ($\beta = 0.5$) pixel by pixel and frame-aligned prior to summing the frames. Isotope images were calculated as $^{12}\text{C}^{13}\text{C}/^{12}\text{C}_2$ and $^{12}\text{C}^{15}\text{N}/^{12}\text{C}^{14}\text{N}$ and expressed relative to the Vienna Pee Dee Belemnite (VPDB) standard as $\delta^{13}\text{C}$ (‰), or relative to air as $\delta^{15}\text{N}$ (‰), respectively. An in-house yeast reference material with known $\delta^{13}\text{C}$ ($-11‰$) and $\delta^{15}\text{N}$ ($+0.4‰$) (James Moran, PNNL, Personal communication) was analyzed during each analytical session to ensure quality control and to calibrate isotope analyses of the PyOM surfaces.

2.10. Data analysis

Langmuir isotherms were fitted to the adsorption data using the following equation:

$$qe = Q_o * K_L * C_e / (1 + K_L * C_e),$$

whereby qe (mg DOC L^{-1}) is the adsorption capacity, C_e (mg DOC L^{-1}) is the equilibrium concentration after adsorption, Q_o (mg DOC g^{-1}) is the maximum sorption capacity of the amendment, and K_L (L mg^{-1}) is a Langmuir constant. Calculations were performed using non-linear regression, and sum of squares (r^2) were calculated using SigmaPlot 12.5 (SAS, Cary, NC).

Respiration data were analyzed using R version 3.3.1 (R Foundation for Statistical Computing, Vienna, Austria). Sample respiration was parsed into PyOM and nSOC-

derived $\text{CO}_2\text{-C}$ using the following equations (Balesdent and Mariotti, 1996):

$$\delta_{\text{measured}} = \delta_{\text{nSOC}}(f_{\text{nSOC}}) + \delta_{\text{PyOM}}(1 - f_{\text{nSOC}})$$

$$f_{\text{nSOC}} = (\delta_{\text{measured}} - \delta_{\text{PyOM}}) / (\delta_{\text{nSOC}} - \delta_{\text{PyOM}})$$

$$f_{\text{nSOC}} \text{CO}_2 - \text{C respired} = \text{respired nSOC}$$

$$\text{CO}_2 - \text{C respired} - \text{respired nSOC} = \text{respired PyOM} - \text{C}$$

$\delta^{13}\text{C}$ of bulk PyOM (δ_{PyOM}) was used as the endmember for isotope partitioning, because bulk PyOM values were previously found to be appropriate proxies for $^{13}\text{CO}_2$ from PyOM (Whitman et al., 2014b). Soil isotope values (δ_{soil}) to be used in isotope partitioning were obtained daily using the average $\delta^{13}\text{C}$ for CO_2 from control treatments. Mean differences were assessed using ANOVA analysis and Tukey corrections for multiple comparisons, as well as two-sample t-tests between individual treatments. Cumulative respiration data were analyzed using pairwise comparisons between treatments based on a mixed effects linear model with a random effect on the sample jar to correct for multiple samplings.

3. RESULTS

3.1. nSOC mineralization

In comparison to perlite and sand, adding PyOM caused rapid reduction in nSOC mineralization (Fig. 1a) and greater cumulative negative priming by day 2, with PyOM additions causing significantly more negative priming than additions of ashed subsoil by day 30 (Fig. 1c). Cumulative nSOC mineralization after perlite addition was significantly lowered only by day 20 ($p < 0.05$), and reductions after sand additions were not significant during the entire observation period. Most of the changes occurred during the first seven days, except after additions of PyOM, which was not only strongest during the first seven days but continued throughout the experiment albeit slower than during the initial period (Fig. 1c).

Adding PyOM pyrolyzed at 450 $^{\circ}\text{C}$ caused a reduction in nSOC mineralization by 0.72 mg $\text{CO}_2\text{-C g}^{-1}$ soil. By comparison, PyOM mineralization was only 0.0076 mg $\text{CO}_2\text{-C g}^{-1}$ soil (purple line without symbols labeled "PyOM respired" in Fig. 1d), which is equivalent to only 1% of the negative priming observed (filled circles symbols labeled "Topsoil+450PyOM" in Fig. 1d).

All PyOM materials added at 10 mg g^{-1} to soil caused negative priming, irrespective of pyrolysis temperature (200–750 $^{\circ}\text{C}$) (Fig. 2a). PyOM pyrolyzed at 750 $^{\circ}\text{C}$ caused the most negative priming (significantly different from control at day 30) followed by those at 600, 200, 300 and 450 $^{\circ}\text{C}$ at days 30, 30, 40, 50, and 60, respectively. Adding 750PyOM resulted in 17% lower cumulative nSOC mineralization than the control at day 60.

Increasing the application rate (0, 0.5, 1, 2.5, 5, 10 mg g^{-1}) significantly changed cumulative nSOC mineralization (main effect $p < 0.05$). However, only PyOM application rates of 10 mg g^{-1} tended ($p < 0.1$) to decrease cumulative nSOC mineralization by 10% at day 35 as compared to

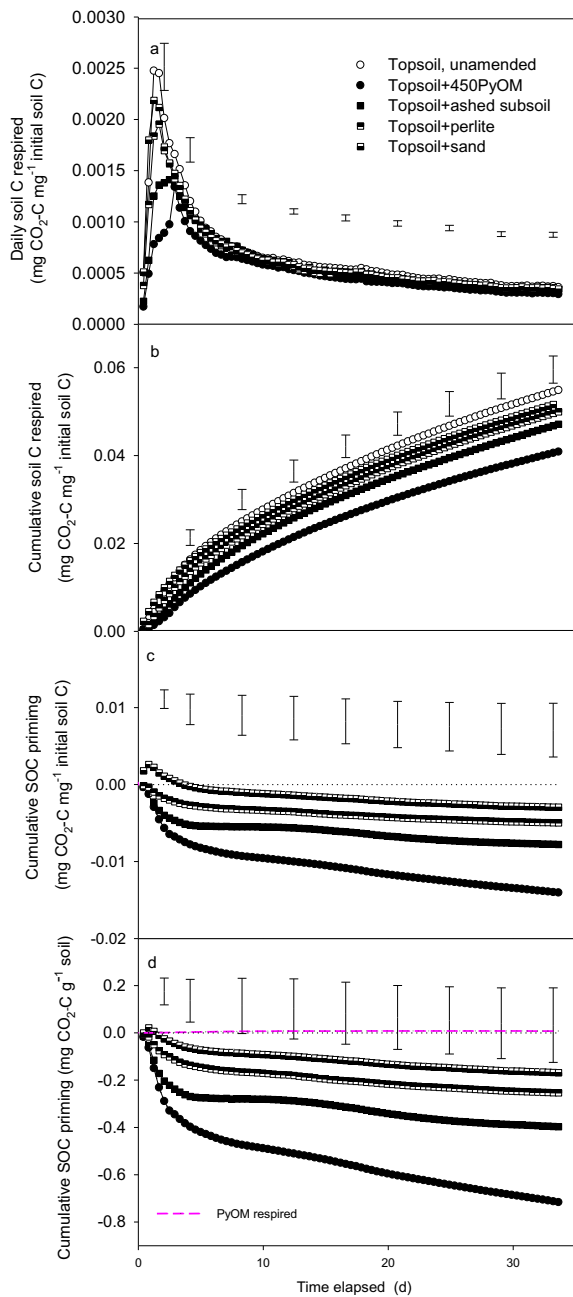


Fig. 1. Mineralization of nSOC and PyOM after additions of either PyOM (10 mg g^{-1}), in comparison to equivalent volume of quartz sand, perlite or ashed subsoil. (a) Mean daily nSOC respired per unit initial C per day, error bars indicate LSD at that timepoint. (b) Mean cumulative nSOC respired per unit initial C. (c) Mean cumulative nSOC priming per unit initial soil mass C. Cumulative priming calculated by subtracting unamended control from treatment value. Dashed line represents unamended soil, data above this line indicate positive priming, below indicate negative priming. (d) Mean cumulative nSOC priming per unit soil mass. Dashed line represents unamended soil, pink solid line indicates PyOM-C respired g^{-1} soil ($n = 5$; bars show least significant difference (LSD) at $p < 0.05$). (For interpretation of the references to colour in this figure legend, the reader is referred to the web version of this article.)

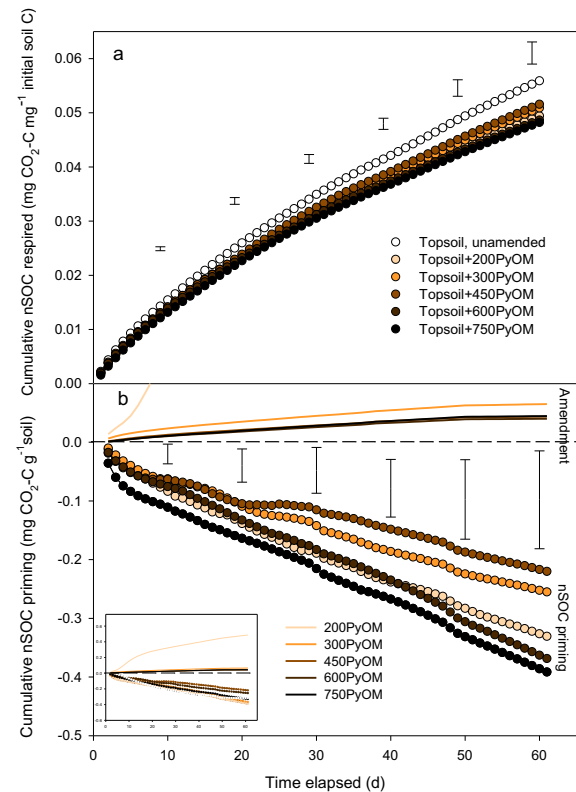


Fig. 2. Cumulative nSOC mineralization after additions of PyOM (10 mg g^{-1} soil) pyrolyzed at different temperatures. (a) Mean cumulative nSOC respiration per unit initial soil C. (b) Mean cumulative priming per unit soil, determined by subtracting unamended control from treatment value. Dashed line represents unamended soil. Solid lines indicate PyOM-C respired. Inset image shows entire range of data ($n = 5$; bars indicate LSD at $p < 0.05$).

the PyOM addition of 1.0 mg g^{-1} ($p < 0.05$). PyOM application rate therefore had no relevant effect on cumulative nSOC mineralization (Fig. 3).

3.2. Microbial biomass

Microbial biomass did not significantly vary between amendments (Fig. 4).

3.3. Adsorption of dissolved organic carbon

PyOM produced at 750°C adsorbed about three times more DOC than that produced at 450°C , the latter causing a maximum adsorption 19 times greater than either soil (Fig. 5; Table 3). PyOM pyrolyzed at 200°C did not adsorb any DOC but rather released DOC into solution, as did the temperate topsoil, while the other PyOMs and the subsoil released DOC only at low DOC equilibrium concentrations below 40.9 mg L^{-1} (450 PyOM) and 2.3 mg L^{-1} (750 PyOM).

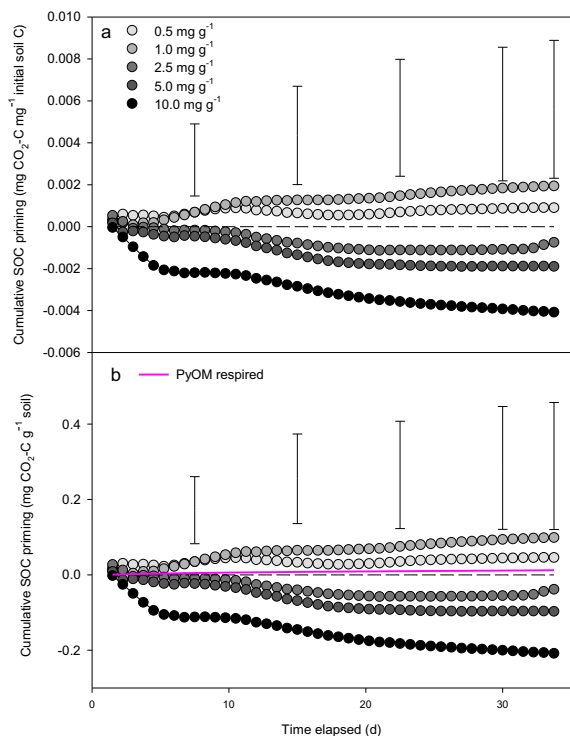


Fig. 3. Cumulative nSOC priming after additions of different rates of PyOM (produced at 450 °C), (a) per unit initial soil C d^{-1} , or (b) g^{-1} soil per day. Dashed horizontal line represents unamended soil. Solid line indicates PyOM-C respiration g^{-1} soil for an application rate of 10 mg g^{-1} ($n = 5$; bars indicate LSD at $p < 0.05$).

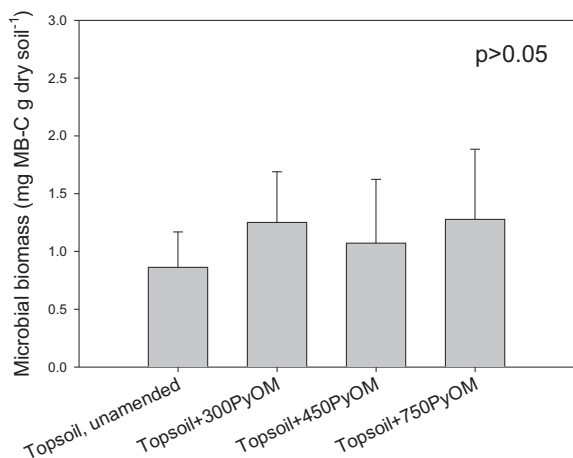


Fig. 4. Microbial biomass (MB) for experiment 2 (means and standard errors; $n = 5$).

3.4. NanoSIMS

Labeled PyOM showed a strong ^{13}C and ^{15}N isotope enrichment using nanoSIMS (Fig. 6). After exposure to soil for 60 d, exterior surfaces of PyOM produced at both 450 °C and 600 °C were covered with unlabeled nSOC in comparison to the original PyOM. This coverage was uneven and showed thicker coatings of unlabeled soil C in

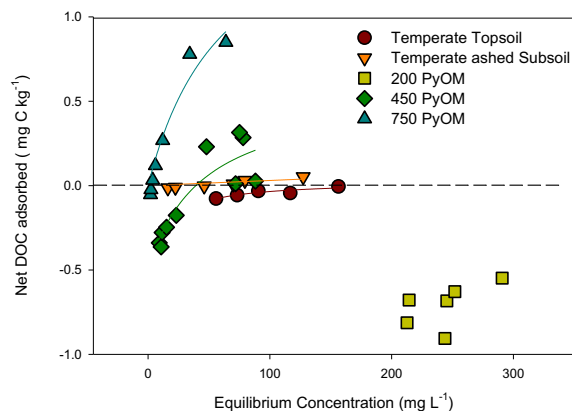


Fig. 5. Adsorption of DOC by PyOM pyrolyzed at 200, 450 and 750 °C in comparison to topsoil and ashed subsoil ($n = 1$).

some locations than others, appearing slightly more heterogeneous on PyOM produced at the higher temperature.

4. DISCUSSION

4.1. Positive and negative priming

We observed positive priming as a result of additions of PyOM at rates less than 2.5 mg g^{-1} to mineral soil over monthly or longer time periods, which has also been seen in other studies (Cross and Sohi, 2011; Jones et al., 2012; Whitman et al., 2014b). At 10 mg g^{-1} soil, the observed negative priming by PyOM of 1–34% across 200–750PyOM in comparison to unamended soil was in the same order of magnitude as reported in the meta-analysis by Maestrini et al. (2015) for similar incubation times. By performing several different types of incubations and analyses, we determined that dilution and sorption were more important than other negative priming mechanisms in our study as discussed below.

4.2. Dilution mechanism

The observation that daily nSOC mineralization from soil amended with PyOM in comparison to different inorganic diluents largely converged by day 7 (Fig. 1a) may indicate that short-term processes dominate nSOC mineralization during that period. The reduced nSOC mineralization after additions of inorganic amendments (Fig. 1b–d) suggests either dilution or adsorption as the mechanism for negative priming, as no organic substrate was added. The low surface area of the added sand with typically low DOC adsorption (Clausen et al., 2001; Kothawala et al., 2008; Liang et al., 1996) suggests that the resultant reductions in nSOC can be mainly explained by dilution, rather than adsorption. Because all amendments were added at the same volume, plotting their reduction in nSOC vs. their surface area allows us to obtain an estimate of the predicted effects of a dilution by that volume, separately from potential surface area effects: extrapolation of decreasing surface area to a hypothetical amendment with no surface area at equivalent volume to the added PyOM (y-intercept on the

Table 3

Adsorption maximum (Q_0), Langmuir constant (K_L) and regression values for DOC adsorption to topsoil, ashed subsoil, and PyOM pyrolyzed at either 200, 450 or 750 °C.

	Q_0 (mg DOC L ⁻¹)	K_L (L mg ⁻¹)	r^2	p-Value
Topsoil	0.02	0.160	0.84	0.0280
Ashed subsoil	0.03	0.470	0.66	0.0497
200PyOM	nd	nd	nd	nd
450PyOM	0.57	0.024	0.79	0.0005
750PyOM	1.80	0.016	0.94	0.0600

nd: not determined as no model could be fitted.

supplementary online Fig. S1; supplementary discussion) indicates a dilution contribution of 1.8 mg CO₂-C g⁻¹C, or 19% of the reductions observed with PyOM pyrolyzed at 450 °C over the first 7 days. This suggests that dilution is an important negative priming mechanism, at least initially, which has so far only been proposed (Whitman et al., 2014b) yet not quantified. Priming studies also with additions of uncharred OM should include dilution as a possible mechanism and the method developed here may be used for its quantification. However, the greater negative priming with PyOM than is explainable by surface area and the continuously lower daily mineralization of nSOC with PyOM additions beyond the first 7 days indicate that surface interactions may be even more important than dilution.

4.3. Substrate switching and co-metabolism

Substrate switching, by definition, can only be equivalent to the amount of PyOM respired (shown as lines without symbols in Figs. 1d, 2b, and 3b) that is then not respired from nSOC. Since much more PyOM is respired (yellow line in the inset of Fig. 2b) than nSOC mineralization is reduced (yellow¹ circle in Fig. 2b), substrate switching may therefore explain up to 100% of the cumulative negative priming observed for PyOM produced at 200 °C, but not more than 24% for the 300PyOM and, on average, not more than 13% for the additions of PyOM produced at higher temperature (Fig. 2). This is consistent with the different fractions of volatile matter in the different PyOMs (Table 1), with 200PyOM having comparatively high concentrations of volatile matter (87%), and higher temperature PyOM having comparatively low concentrations of volatile matter. Mineralization of PyOM (at 450 °C, with volatile matter of 24%) as a proportion of reductions in nSOC mineralization (i.e., negative priming) that can be interpreted as substrate switching, were as low as 1% (Fig. 1). In addition, PyOM produced at the highest tested temperature of 750 °C (with 10% volatile concentration) contributed little to microbial biomass (0.07%), had very little mineralizable C, and, especially between day 40–60, mineralized only 0.0076 mg CO₂-C g⁻¹ soil d⁻¹, which was far below the continued daily reduction of nSOC mineralization of 0.12 mg CO₂-C g⁻¹ soil d⁻¹. Thus, while substrate

switching could explain part of the negative priming for the low-temperature PyOM, it is likely negligible for the higher-temperature PyOM.

Co-metabolism did not cause a significant net increase in nSOC mineralization with any of the tested PyOM. This, however, is not sufficient evidence to conclude that co-metabolism did not occur but merely indicates that it was less important than the sum of all negative priming mechanisms together. Co-metabolism may, similar to substrate switching, only occur simultaneously with CO₂ production from the added substrate (Blagodatskaya and Kuzyakov, 2008). Using the occurrence of a correlation between 24-hour-mineralization of PyOM and nSOC mineralization as the criterion (Fig. 7), our data indicate that co-metabolism may have occurred early in the incubation, but could not be detected at or beyond 40 days, when daily PyOM mineralization decreased to less than 12% of the daily reduction in nSOC mineralization.

4.4. Inhibition

Microbial biomass did not decrease with PyOM additions, suggesting that inhibition of the microbial community did not play an important role in explaining negative priming. It should be kept in mind that our measurements may have underestimated total microbial biomass with PyOM additions in comparison to no additions, because no adjustments were made for a greater adsorption of any organic matter released from lysed cells during fumigation to the PyOM than the soil, as suggested by the greater DOC adsorption to PyOM than soil (Fig. 5). This would have resulted in an underestimation of the amount of microbial biomass in the presence of PyOM for fresh and aged PyOM (Dai et al., 2017; Liang et al., 2010). However, despite this potential methodological issue, if PyOM was indeed adsorbing additional MB-C, that would indicate that the initial microbial biomass was actually higher in PyOM treatments, further supporting a lack of microbial inhibition. One can assume that if the added PyOM was killing microbes (and thus causing negative priming due to a lower population of respiring organisms) the microbial biomass would be less than in the unamended control. This mechanism was tested in this study by excluding changes induced as part of varying pH, water or nutrient availability, as these were all controlled. This result corroborates earlier studies that also did not find inhibition due to organic or non-nutrient inorganic compounds in PyOM (Bruun et al., 2008; Kolb et al., 2009; Maestrini et al., 2014).

¹ For interpretation of color in Fig. 2, the reader is referred to the web version of this article.

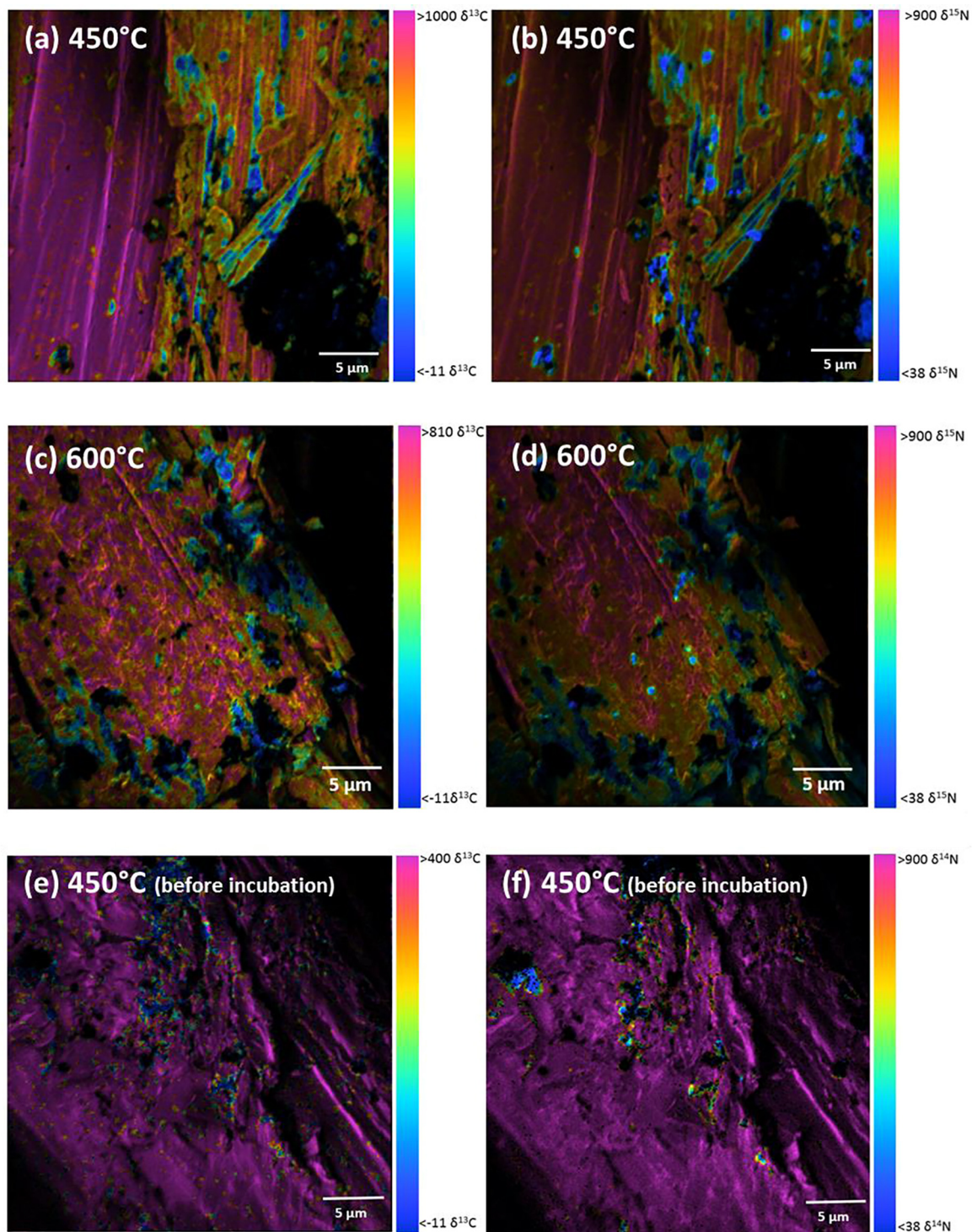


Fig. 6. Distribution of ^{13}C (a, c) and ^{15}N (b, d) isotopes of PyOM particles produced at 450 °C (a, b) or 600 °C (c, d) using nanoSIMS analyses isolated from soil after incubation (see method for isolation procedure) in comparison to the original PyOM shown for 450 °C (e, f); bright pink colors indicate enriched material reminiscent of the original PyOM and blue colors indicate natural abundance materials from nSOC. (For interpretation of the references to colour in this figure legend, the reader is referred to the web version of this article.)

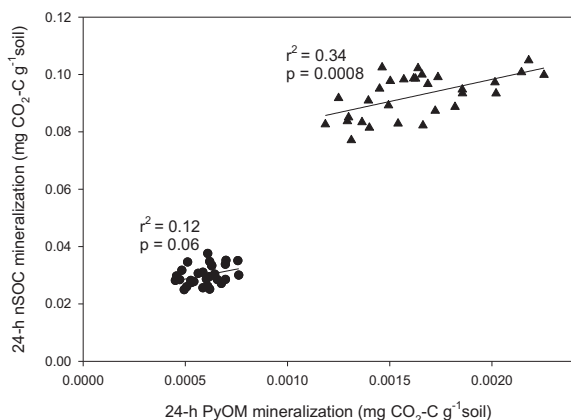


Fig. 7. Mineralization of nSOC over 24 h plotted against PyOM mineralization over the same time period at day 3 (triangles) and day 40 (circles) of Experiment 2 shown in Fig. 2. PyOM produced at 300, 450, 600 and 750 °C included in regression ($n = 5$).

4.5. Adsorption

Greater adsorption of DOC to PyOM than to soil can quantitatively explain the lower mineralization of nSOC in the presence of PyOM in our study. Sorption has been proposed as a likely mechanism by several authors (Cross and Sohi 2011; Kuzyakov et al., 2009; Maestrini et al., 2014; Whitman et al., 2014b; Woolf and Lehmann, 2012; Zimmerman et al., 2011) due to PyOM's often high surface area, porosity, charge, and overall highly adsorptive characteristics (Ahmad et al., 2013). Significant removal of DOC of 26–52% by PyOM was also reported in organic horizons (Pietikäinen et al., 2000). Our adsorption isotherms showed 19-times greater DOC sorption to the 450PyOM than to the ashed subsoil and an even greater sorption than to the topsoil. The 750PyOM was capable of adsorbing 3 times more DOC than the 450PyOM, but only produced about 1.8 times more negative priming than the 450PyOM. The lower reduction in nSOC mineralization compared to the increase in DOC adsorption could be caused by the vast differences in experimental practice. In the adsorption experiment, DOC, soil and PyOM were all freely suspended in water where they could easily interact, whereas in the incubation, although the soils were moist, there would have been much less mobility of DOC and nSOC and therefore overall less interaction. However, the comparison illustrates that adsorption is quantitatively a likely process.

The decrease in nSOC mineralization with greater conversion temperature may provide a further argument for adsorption as the main mechanism promoting negative priming in this study even with PyOM produced at low temperature: the decrease in mineralizable C from PyOM produced at 450 °C compared to 750 °C was far less than the reduction in nSOC mineralization and reduction in volatile matter. Therefore, adsorption may be underestimated as a process for reducing nSOC mineralization at lower pyrolysis temperature.

Our nanoSIMS data also supported the proposition that nSOC was adsorbed on the surfaces of PyOM. The 450 and 600PyOM both showed natural abundance $\delta^{13}\text{C}$ values on

the surface of the highly labeled PyOM, indicating that nSOC was indeed present on PyOM surfaces. Whether this co-location of PyOM and nSOC actually led to interactions and how strong these were cannot be discerned by nanoSIMS. The patchiness and apparent accrual of SOC in micrometer-sized cavities on PyOM surfaces may indicate sorption in excess of a monolayer. The accrual of nSOC along discernable morphological features of the PyOM may serve as an indication of sorption mechanisms that are not random. Whether such patchiness is a result of the surface morphology (e.g., entrapment of nSOC in large pores) or variations in charge properties as observed on mineral surfaces (Vogel et al., 2014) is not clear and would be an intriguing subject of future investigation.

4.6. Comparison of mechanisms

Using the data from this suite of experiments, we suggest that the most likely mechanism of the negative priming observed is sorption, with dilution also being a significant contributor during the first week. We further suggest that substrate switching and inhibition mechanisms do not contribute significantly to negative priming interactions. Although we did observe substrate switching, this only accounted for 1% of negative priming with dilution explaining 19% (Supplementary Fig. S2). The majority of the remaining negative priming (80%) may be due to adsorption, based on our adsorption isotherm assay and supported by nanoSIMS observations. Unlike substrate switching, adsorption interactions between PyOM and nSOC may be more long-lasting, with net negative priming continuing for a longer period of time (Woolf and Lehmann 2012; Zimmerman et al., 2011). The continuation of this negative priming may be limited by adsorption sites, but it is not known if saturation of these sites will eventually limit negative priming by adsorption. Because the isotherms indicate a several-fold greater maximum potential adsorption than observed emission reductions of SOC after 60 days, one may expect negative priming by adsorption to continue for some time. The negative priming observed 7–9 years after PyOM addition (Dharmakeerthi et al., 2015; Weng et al., 2017) and in PyOM-rich Amazonian Dark Earths that are several thousand years old (Liang et al., 2010) suggests that negative priming may continue for years to millennia after PyOM input. Although additional adsorption on PyOM surfaces may continue for some time including pore filling, it is not certain that adsorption is sufficient to explain the accrual of nSOC over years to millennia, since adsorption of DOC (as seen in Fig. 5 for relatively short-term batch experiments) must be limiting negative priming eventually. Whether PyOM effects on aggregation (Obia et al., 2016), signaling between microorganisms (Masiello et al., 2013) or electrochemical processes (Sun et al., 2017) play a role for priming in the presence of PyOM remains to be quantified.

Positive priming through co-metabolism is also occurring early in the incubation with up to 38% short-term increase in nSOC mineralization (which increases the gross effect of negative priming by adsorption by an equivalent proportion), but is overwhelmed by negative priming over

time. The relative importance of different mechanisms responsible for negative priming, as summarized here for PyOM pyrolyzed at 450 °C (Supplementary Fig. S2), will vary with PyOM properties, as shown here and in other studies (Zimmerman et al., 2011), and also with soil type and SOC properties (Whitman et al., 2014b).

5. CONCLUSION

Dilution accounted for a significant portion of negative priming, but adsorption is the most likely explanation for the majority of negative priming by addition of PyOM observed in this study for PyOM produced at 300 °C and above. Substrate switching was able to explain reductions in nSOC mineralization after additions of weakly charred (200PyOM) OM. Sorption of nSOC on PyOM surfaces has the potential for long-term carbon storage, as the nSOC is bound to the surface of persistent PyOM and may thereby be protected from mineralization. Given that PyOM naturally exists widely in soils, and fires are expected to increase in the future in many ecosystems (Santín et al., 2016), these results indicate that priming should be incorporated in biochar management decisions and accounted for in carbon cycling models. Except for adsorption, these mechanisms may also be important for additions of uncharred organic matter. Especially dilution should be included in future studies of priming by charred and uncharred OM additions using the method developed here. In order to correctly parameterize such models, more long-term studies and field experiments with and without plants must be conducted to ensure that our results are representative of real-world PyOM-nSOC interactions. The fate of adsorbed nSOC should be further examined, as it is not clear whether adsorption of microbial or plant matter constitutes the bulk of the retained nSOC, and whether eventual desorption or in-situ mineralization may remobilize it, reversing the negative priming observed here.

ACKNOWLEDGEMENTS

Funding from United States Department of Agriculture (USDA) National Institute of Food and Agriculture (NIFA) (award no. #2014-67003-22069), USDA Hatch, and the Department of Soil and Crop Science at Cornell University is gratefully acknowledged. Measurements at the Environmental Molecular Sciences Laboratory (EMSL) were supported by the Department of Energy (UP 47803). Thanks to Kelly Hanley, Erika Mudrak and John Cliff for analytical and logistical support.

REFERENCES

Abatzoglou J. and Williams A. (2016) Impact of anthropogenic climate change on wildfire across western US forests. *Proc. Nat. Acad. Sci.* **113**, 11770–11775.

Ahmad M., Rajapaksha A. U., Lim J. E., Zhang M., Bolan N., Mohan D., Vithanage M., Lee S. S. and Ok Y. S. (2013) Biochar as a sorbent for contaminant management in soil and water: a review. *Chemosphere* **99**, 19–33.

Balesdent J. and Mariotti A. (1996) Measurement of soil organic matter turnover using ¹³C natural abundance. In *Mass Spec-*

trometry of Soils (eds. T. W. Boutton and S. I. Yamasaki). CRC Press/Taylor and Francis, Boca Raton, pp. 83–111.

Bingeman C. W., Varner J. E. and Martin W. P. (1953) The effect of the addition of organic materials on the decomposition of an organic soil. *Soil Sci. Soc. Am. J.* **17**, 34–38.

Bird M. L., Wynn J. G., Saiz G., Wurster C. M. and McBeath A. (2015) The pyrogenic carbon cycle. *Ann. Rev. Earth Plan. Sci.* **43**, 273–298.

Black C., Evals D., White J., Ensminger L. and Clark F. (1965) Physical and mineralogical properties, including statistics of measurement and sampling. *Methods of Soil Analysis Part 1*. American Society of Agronomy, Number 9 in Agronomy Series, Madison, WI.

Blagodatskaya E. and Kuzyakov Y. (2008) Mechanisms of real and apparent priming effects and their dependence on soil microbial biomass and community structure: critical review. *Biol. Fert. Soils* **45**, 115–131.

Boodley J. W. and Sheldrake R. (1972) *Cornell peat-lite mixes for commercial growing* Information Bulletin No. 43, Cooperative Extension. New York State College of Agriculture and Life Sciences, Cornell University.

Bruun S., Jensen E. S. and Jensen L. S. (2008) Microbial mineralization and assimilation of black carbon: dependency on degree of thermal alteration. *Org. Chem.* **39**, 839–845.

Bruuslema T. and Duxbury J. (1996) Simultaneous measurement of soil microbial nitrogen, carbon, and carbon isotope ratio. *Soil Sci. Soc. Am. J.* **60**, 1787–1791.

Ciais P., Sabine C., Bala G., Bopp L., Brovkin V., Canadell J., Chhabra A., DeFries R., Galloway J., Heimann M., Jones C., Le Quéré C., Myneni R. B., Piao S. and Thornton P. (2013) Carbon and other biogeochemical cycles. In *Climate Change 2013: The Physical Science Basis. Contribution of Working Group I to the Fifth Assessment Report of the Intergovernmental Panel on Climate Change* (eds. T. F. Stocker, D. Qin, G.-K. Plattner, M. Tignor, S. K. Allen, J. Boschung, A. Nauels, Y. Xia, V. Bex and P. M. Midgley). Cambridge University Press, Cambridge, United Kingdom and New York, NY, USA, pp. 465–570.

Clausen L., Fabricius I. and Madsen L. (2001) Adsorption of pesticides onto quartz, calcite, kaolinite, and α -alumina. *J. Environ. Qual.* **30**, 846–857.

Cross A. and Sohi S. P. (2011) The priming potential of biochar products in relation to labile carbon contents and soil organic matter status. *Soil Biol. Biochem.* **43**, 2127–2134.

Dai Z., Webster T. M., Enders A., Hanley K., Xu J., Thies J. E. and Lehmann J. (2017) DNA extraction efficiency from soil as affected by pyrolysis temperature and extractable organic carbon of high-ash biochar. *Soil Biol. Biochem.* **115**, 129–136.

Dharmakeerthi R. S., Hanley K., Whitman T., Woolf D. and Lehmann J. (2015) Organic carbon dynamics in soils with pyrogenic organic matter that received plant residue additions over seven years. *Soil Biol. Biochem.* **88**, 268–274.

Enders A. and Lehmann J. (2012) Comparison of wet digestion and dry ashing methods for total elemental analysis of biochar. *Commun. Soil Sci. Plant Anal.* **43**, 1042–1052.

Enders A., Hanley K., Whitman T., Joseph S. and Lehmann J. (2012) Characterization of biochars to evaluate recalcitrance and agronomic performance. *Biores. Technol.* **114**, 644–653.

Fang Y., Singh B. and Singh B. P. (2015) Effect of temperature on biochar priming effects and its stability in soils. *Soil Biol. Biochem.* **80**, 136–145.

Graber E. R., Singh B., Hanley K. and Lehmann J. (2017) Determination of cation exchange capacity in biochar. In *Biochar: A Guide to Analytical Methods* (eds. B. Singh, M. Camps-Arbestain and J. Lehmann). CRC Press/Taylor and Francis, Boca Raton, FL, pp. 74–84.

- Guerena D., Lehmann J., Thies J., Enders A., Karanja N. and Neufeldt H. (2015) Partitioning the contributions of biochar properties to enhanced biological nitrogen fixation in common bean (*Phaseolus vulgaris*). *Biol. Fert. Soils* **50**, 79–491.
- Jenkinson D. S., Brookes P. C. and Powlson D. S. (2004) Measuring soil microbial biomass. *Soil Biol. Biochem.* **46**, 5–7.
- Jones D. L., Rousk J., Edwards-Jones G., DeLuca T. H. and Murphy D. V. (2012) Biochar-mediated changes in soil quality and plant growth in a three year field trial. *Soil Biol. Biochem.* **45**, 113–124.
- Keith A., Singh B. and Dijkstra F. A. (2015) Biochar reduces the rhizosphere priming effect on soil organic carbon. *Soil Biol. Biochem.* **88**, 372–379.
- Keith A., Singh B. and Singh B. P. (2011) Interactive priming of biochar and labile organic matter mineralization in a smectite-rich soil. *Environ. Sci. Technol.* **45**, 9611–9618.
- Kettler T. A., Doran J. W. and Gilbert T. L. (2001) Simplified method for soil particle-size determination to accompany soil quality analysis. *Soil Sci. Soc. Am. J.* **65**, 849–852.
- Kolb S. E., Fermanich K. J. and Dornbush M. E. (2009) Effect of charcoal quantity on microbial biomass and activity in temperate soils. *Soil Sci. Soc. Am. J.* **73**, 1173–1181.
- Kothawala D. N., Moore T. R. and Hendershot W. H. (2008) Adsorption of dissolved organic carbon to mineral soils: a comparison of four isotherm approaches. *Geoderma* **148**, 43–50.
- Kuzyakov Y. (2010) Priming effects: Interactions between living and dead organic matter. *Soil Biol. Biochem.* **42**, 1363–1371.
- Kuzyakov Y., Subbotina I., Chen H., Bogomolova I. and Xu X. (2009) Black carbon decomposition and incorporation into soil microbial biomass estimated by ¹⁴C labeling. *Soil Biol. Biochem.* **41**, 210–219.
- Liang B. C., Gregorich G., Schnitzer M. and Schulten H.-R. (1996) Characterization of water extracts of two manures and their adsorption on soils. *Soil Sci. Soc. Am. J.* **60**, 1758–1763.
- Liang B., Lehmann J., Sohi S., Thies J., O'Neill B., Trujillo L., Gaunt J., Solomon D., Grossman J., Neves G. and Luizão J. (2010) Black carbon affects the cycling of non-black carbon in soil. *Org. Geochem.* **41**, 206–213.
- Laird D. A. (2008) The charcoal vision: a win-win-win scenario for simultaneously producing bioenergy, permanently sequestering carbon, while improving soil and water quality. *Agron. J.* **100**, 178–181.
- Lehmann J., Skjemstad J. O., Sohi S., Carter J., Barson M., Falloon P., Coleman K., Woodbury P. and Krull E. (2008) Australian climate-carbon cycle feedback reduced by soil black carbon. *Nature Geosci.* **1**, 832–835.
- Lehmann J., Rillig M., Thies J., Masiello C. A., Hockaday W. C. and Crowley D. (2011) Biochar effects on soil biota – a review. *Soil Biol. Biochem.* **43**, 1812–1836.
- Luo Y., Durenkamp M., De Nobili M., Lin Q. and Brookes P. C. (2011) Short term soil priming effects and the mineralisation of biochar following its incorporation to soils of different pH. *Soil Biol. Biochem.* **43**, 2304–2314.
- Masiello C., Chen Y., Gao X., Lui S., Cheng H., Bennett M., Rudgers J., Wagner D., Zygourakis K. and Silberg J. (2013) Biochar and microbial signaling: production conditions determine effects on microbial communication. *Environ. Sci. Technol.* **47**, 11498–11503.
- Maestrini B., Herrmann A. M., Nannipieri P., Schmidt M. W. I. and Abiven S. (2014) Ryegrass-derived pyrogenic organic matter changes organic carbon and nitrogen mineralization in a temperate forest soil. *Soil Biol. Biochem.* **69**, 291–301.
- Maestrini B., Nannipieri P. and Abiven S. (2015) A meta-analysis on pyrogenic organic matter induced priming. *Global Change Biol. Bioenergy* **7**, 577–590.
- Nelson D. W. and Sommers L. E. (1996) *Total carbon, organic carbon and organic matter*, third ed. SSSA. Book Ser. 5. SSSA, Madison, WI, pp. 961–1010.
- Obia A., Mulder J., Martinsen V., Cornelissen G. and Børresen T. (2016) In situ effects of biochar on aggregation, water retention and porosity in light-textured tropical soils. *Soil Till. Res.* **155**, 35–44.
- Pietikäinen J., Kiikkilä O. and Fritze H. (2000) Charcoal as a habitat for microbes and its effect on the microbial community of the underlying humus. *Oikos* **89**, 231–242.
- Santín C., Doerr S. H., Kane E. S., Masiello C. A., Ohlson M., Rosa J. M., Preston C. M. and Dittmar T. (2016) Towards a global assessment of pyrogenic carbon from vegetation fires. *Glob. Change Biol.* **22**, 76–91.
- Singh B., Dolk M. M., Shen Q. and Camps-Arbestain M. (2017) Biochar pH, electrical conductivity and liming potential. In *Biochar: A Guide to Analytical Methods* (eds. B. Singh, M. Camps-Arbestain and J. Lehmann). CRC Press, Taylor and Francis, Boca Raton, FL, pp. 23–38.
- Stockmann U., Adams M. A., Crawford M. A., Field D. J., Henakaarchchi N., Jenkins M., Minasny B., McBratney A. B., de Remy de Courcelles V., Singh K., Wheeler I., Abbott L., Angers D. A., Baldock J., Bird M., Brookes P. C., Chenu C., Jastrow J. D., Lal R., Lehmann J., O'Donnell A. G., Parton W. J., Whitehead D. and Zimmermann M. (2013) The knowns, known unknowns and unknowns of sequestration of soil organic carbon. *Agric. Ecosyst. Environ.* **164**, 80–99.
- Sun T., Levin B. D. A., Guzman J. J. L., Enders A., Muller D. A., Angenent L. T. and Lehmann J. (2017) Rapid electron transfer by the carbon matrix in natural pyrogenic carbon. *Nature Commun.* **8**, 14873.
- Vance E. D., Brookes P. C. and Jenkinson D. S. (1987) Microbial biomass measurements in forest soils: the use of the chloroform fumigation-incubation method in strongly acid soils. *Soil Biol. Biochem.* **19**, 697–702.
- Vogel C., Mueller C. W., Höschel C., Buegger F., Heister K., Schulz S., Schlöter M. and Kögel-Knabner I. (2014) Submicron structures provide preferential spots for carbon and nitrogen sequestration in soils. *Nature Commun.* **5**, 2947.
- Wang J., Xiong Z., Yan X. and Kuzyakov Y. (2016) Carbon budget by priming in a biochar-amended soil. *Eur. J. Soil Biol.* **76**, 26–34.
- Wardle D. A., Nilsson M. C. and Zackrisson O. (2008) Fire-derived charcoal causes loss of forest Humus. *Science* **320**, 629.
- Weng Z. H., Van Zwieten L., Singh B. P., Tavakkoli E., Joseph S., Macdonald L. M., Rose T. J., Rose M. T., Kimber S. W., Morris S. and Cozzolino D. (2017) Biochar built soil carbon over a decade by stabilizing rhizodeposits. *Nature Clim. Change* **7**, 371–376.
- Whitman T., Zimmerman A. and Singh B. P. (2015) Priming effects in biochar-amended soils: Implications of biochar soil organic matter interactions for carbon storage. In *Biochar for Environmental Management: Science, Technology and Implementation* (eds. J. Lehmann and S. Joseph). Routledge, London, pp. 455–488.
- Whitman T., Enders A. and Lehmann J. (2014a) Pyrogenic carbon additions to soil counteract positive priming of soil carbon mineralization by plants. *Soil Biol. Biochem.* **73**, 33–41.
- Whitman T., Zhu Z. and Lehmann J. (2014b) Carbon mineralizability determines interactive effects on mineralization of pyrogenic organic matter and soil organic carbon. *Environ. Sci. Technol.* **48**, 13727–13734.
- Williams A. P. and Abatzoglou J. T. (2016) Recent advances and remaining uncertainties in resolving past and future climate effects on global fire activity. *Curr. Clim. Change Rep.* **2**, 1–14.

- Witt C., Gaunt J., Galicia C., Ottow J. and Neue H. (2000) A rapid chloroform-fumigation extraction method for measuring soil microbial biomass carbon and nitrogen in flooded rice soils. *Biol. Fert. Soils* **30**, 510–519.
- Woolf D. and Lehmann J. (2012) Modelling the long-term response to positive and negative priming of soil organic carbon by black carbon. *Biogeochem.* **111**, 83–95.
- Zimmerman A. R., Gao B. and Ahn M. Y. (2011) Positive and negative carbon mineralization priming effects among a variety of biochar-amended soils. *Soil Biol. Biochem.* **43**, 1169–1179.

Associate editor: Owen Duckworth